Computers and Electronics in Agriculture 187 (2021) 106311

Contents lists available at ScienceDirect

Computers and Electronics in Agriculture

journal homepage: www.elsevier.com/locate/compag

Original papers

Robotics-based vineyard water potential monitoring at high resolution

Verónica Saiz-Rubio [a], Francisco Rovira-Más [a,*], Andrés Cuenca-Cuenca [a], Fernando Alves [b]

[a] Agricultural Robotics Laboratory (ARL), Universitat Politècnica de València, Camino de Vera s/n, 46022 Valencia, Spain
[b] Symington Family Estates, Vinhos SA, Travessa Barão de Forrester 86, 4431-901 Vila Nova de Gaia, Portugal

ARTICLE INFO

Keywords:
Precision Agriculture
PRI
Plant water potential
Proximal sensing
Autonomous Ground Vehicle (AGV)

ABSTRACT

The purpose of this research is deploying a proximal sensing solution using non-invasive and cost-effective sensors onboard an Autonomous Ground Vehicle (AGV) as a feasible way for building high-resolution maps of water potential in vineyards. The final objective is offering growers a practical system to make decisions about water management, especially for arid climatic conditions. The monitoring AGV was entirely developed within this research context, and as a result, it is a machine specifically designed to endure off-road conditions and harsh environments. The autonomous vehicle served as a massive, non-invasive, and on-the-go data collector robotic platform. The sensors used for measuring the relevant field variables were two spectral reflectance sensors (SRS), an infrared radiometer, and an on-board weather sensor. The collected data were displayed on comprehensible grid maps using the Local Tangent Plane (LTP) coordinate system. The proposed model has a coefficient of determination R^2 of 0.69, and results from combining six parameters: the canopy and air temperatures (as the temperature difference), the relative humidity, the altitude difference, the Normalized Difference Vegetation Index (NDVI), and the Photochemical Reflectance Index (PRI). The strongest relationships found in this study were between the temperature difference and PRI, with an R^2 of 0.75, and the temperature difference with the leaf water potential with an R^2 of 0.61. The practical use of these high-resolution maps includes irrigation scheduling and harvest zoning for sorting grape quality, with a further use as inputs to complex artificial intelligence algorithms considering larger areas or complementing airborne data. Future improvements to make the models more robust and versatile will entail considering additional variables, locations, or grapevine cultivars, and even other crops grown in vertical trellis systems.

1. Introduction

Climate change has been sometimes denied, but the reality inferred from data seems clear as more research is available every year: climate conditions nowadays are different compared to a few decades ago. Increasing temperatures are affecting different sectors, being agriculture one of the sectors mostly affected by its consequences, since plant growth depends directly on the ambient conditions. Significant changes in ambient temperatures have made that some wineries like Bodegas Torres (Fernandez Esteban, 2019) buy fields at higher (cooler) latitudes in Spain. Similarly, not only temperatures, but also the availability of water, made Spottswoode Estate Vineyard and Winery, in California (USA), experiment with new vine varieties to find new ways of maximizing water use, as their vines were found to be at risk of collapse in the ripening and maturation periods (Della Cava, 2019).

Optimizing the use of water for agriculture has become increasingly important due to the consequences of climate change, which are leading to more frequent droughts, heat waves, or alteration of the precipitation patterns (Fraga et al., 2017; Jones and Alves, 2012; Ortuani et al., 2019; Santos et al., 2020). As a result, any task related to save water will be crucial, and acquiring new habits for the growers in regular irrigation practices will be needed. Ortuani et al. (2019) have demonstrated that varying irrigation practices such as variable-rate drip irrigation can lead to reductions of water use by 18%, compared to the regular irrigation practices made by the owner in a commercial vineyard, without losses in yield and berry quality, and even resulting in a more homogeneous grape maturation in time. Some concerns, however, have been claimed by wine producers regarding such water-saving policies, on the hypothesis that the key attributes of the final wine can be affected by these irrigation practices. Intrigliolo et al. (2008) found large differences in the wine components (also in the grapes and must) between non-irrigated and irrigated vines, but there were practically no differences among vines with slightly different irrigation rates, this is, irrigating one group of plants at 100% of the estimated crop evapotranspiration (ETc)

* Corresponding author.
E-mail addresses: vesairu@upv.es (V. Saiz-Rubio), frovira@upv.es (F. Rovira-Más).

https://doi.org/10.1016/j.compag.2021.106311
Received 16 March 2021; Received in revised form 29 June 2021; Accepted 2 July 2021
Available online 13 July 2021

until harvest, and another group of plants at 50% ETc until veraison and then at 100% ETc thereafter. This result provides evidence to decrease high irrigation rates with the purpose of optimizing water use for vegetation, but it also requires knowing how much water is adequate for each vine to produce at its highest potential. This information turns key for those winemakers that stress their vines at late phenological stages to get wines of higher quality, as severe water deficits can make the plants reach the permanent wilting point. In vineyards that are not flat, when basins form within the field, water tends to accumulate in the soil, and this water reserve can reach up to 50% for some kinds of soil. This phenomenon has been observed in the testing field for the present research in Portugal, and it had already been noticed in Spain. The altitude difference influences the water status of plants due to this water reserve, which further depends on rain and runoff (Rovira-Más and Sáiz-Rubio, 2013). Due to its robustness, the predominant method to assess plant water status in viticulture has been through the measurement of the plant water potential with a pressure chamber, originally developed by Scholander et al. in 1965 (Rienth and Scholasch, 2019). The plant water potential, despite being one of the parameters mostly used in irrigation monitoring (Santesteban et al., 2011; Tysseyre et al., 2005), implies using a methodology that is slow, destructive, with limited temporal and spatial resolution (Ihuoma and Madramootoo, 2017), and requiring excessive labor efforts, which often results tedious as operators need to carry heavy equipment under the strong midday sun of the summer. The present research study uses the hand-held pressure chamber for ground truth validation, but it aims, precisely, at developing a valid, rapid, objective, and non-invasive alternative to consistently determine grapevine water status.

Several indices have been reported to be good indicators for detecting water stress. The photochemical reflectance index, or PRI (Gamon et al., 1997), is one of them, and it was considered in this approach because the sensor measuring it, portable, small, and cost-effective, was suitable for being integrated in a ground robot, as required for this application. The PRI has been considered an early indicator of water stress (Evain et al., 2004; Ihuoma and Madramootoo, 2017; Suárez et al., 2009; Thenot et al., 2002; Williams, 2010), and thus, it can contribute to characterize vine water status (González-Flor et al., 2019). The fact that changes in physiological indicators of water stress and PRI showed stronger correlations at canopy level (Yang et al., 2019), makes this index even more interesting for the present study, as the on-board sensors were close to the canopy and pointing at the vine leaves. The normalized difference vegetation index (NDVI), the best-known index used as a numerical indicator of vegetation greenness, has been also used for irrigation scheduling (Ihuoma & Madramootoo, 2017), or some of its variants, like the Normalized Reference Index (Pôças et al., 2017). Apart from the PRI and the NDVI, Cohen et al. (2005) corroborated that leaf temperature can be used as an indicator of the leaf stomatal conductance and plant water stress, as the increase in plant water stress is linked to leaf stomatal closure and implies a rise in leaf temperature. Guisard (2009) extended this relationship to a canopy level by addressing the canopy temperature as an indicator of water stress in grapevines. In order to normalize the canopy temperature so that the physiological effect of stomatal dynamics on the canopy heat balance can be separated from the physical effects of radiation, convection, and vapor pressure (Testi et al., 2008), the difference between canopy temperature and air temperature was proposed as a water stress indicator instead of just canopy temperature (Idso et al., 1981).

The measurement of the crop indicators described above has typically implied high physical efforts and labor demands, especially for growers applying the principles of Precision Agriculture, or specifically for this context, Precision Viticulture. However, the promising alliance of agriculture and robotics can make that regular field operations result more efficient and less physically-demanding for producers by introducing robotic platforms to perform multiple tasks (Fountas et al., 2020; Saiz-Rubio et al., 2015; Saiz-Rubio & Rovira-Más, 2020; Sarri et al., 2020). Despite the availability of numerous studies proposing alternatives to measure vineyard water status, no solutions have been found for non-invasive monitoring from an autonomous ground vehicle to assist vineyard growers with routine tasks as irrigation and harvesting. Suárez et al. (2008) studied PRI as an indicator of water stress via airborne imaging techniques, but the advantage of monitoring water status from an Autonomous Ground Vehicle (AGV), as proposed in this work, rests on the field of view, which guarantees that only the region of interest is being measured with no interference of soil or weeds, and on the fact that climatic parameters are measured at vine level.

The purpose of this paper is to present and evaluate a practical methodology for the cost-effective monitoring of water status in vineyards. The solution envisioned involves obtaining high resolution maps of water potential to help growers in decision-making processes related to irrigation and harvesting. Water potential is estimated from a proposed mathematical model that combines ambient and crop parameters, using a robot (AGV) for the massive and on-the-go data collection from non-invasive sensors.

2. Materials and methods

2.1. Description of the AGV and its on-board field sensors.

Fig. 1 illustrates the main components of the AGV. Its external dimensions are 1 m wide, 1.2 m long, and 1.2 m tall with the GPS antenna folded, and a mass of approximately 200 kg. The robot is powered by a stack of three Li-ion batteries (EasyBlade 24, VARTA Storage GmbH, Nördlingen, Germany) providing 25.9 V and 192 Ah. The AGV can be handled with a joystick for loading, unloading, and mission placement, being the human-robot interaction established through a Graphic User Interface (GUI) as well as a set of different color lights, such as the *mode indicator* of Fig. 1 that indicates if the AGV is in autonomous mode (orange), manual mode (blue), or in stand-by mode (green). The robot incorporates head and rear lights to ease manual maneuvers with low illumination because it can also navigate at night.

The navigation approach utilized by the AGV to autonomously travel along the vineyard rows is based on local perception. The system uses a 3D sensor (O3M150, ifm electronic GmbH, Essen, Germany) combined with a non-rotational lidar rangefinder (Multi-Ray LED Scanner OMD8000-R2100-R2-2 V1, Pepperl + Fuchs, Mannheim, Germany), and four ultrasonic sensors (UC2000 30GM IUR2 V15, Pepperl + Fuchs, Mannheim, Germany). The central computer on-board the robot includes a fanless processor (IRTBPCFNLALD9H, Irontech, Gerona, Spain) that manages the sensors through a data acquisition card (NI USB-6216, National Instruments, Austin, Texas, USA). The explanation of this navigation system falls outside the scope of this article, but a detailed description is available in Rovira-Más et al. (2020). The AGV is programmed to apply safety measures in case of unexpected situations, stopping and releasing an acoustic signal when it encounters an obstacle in the middle of the row. It also incorporates a safety bumper that cuts the tractive power immediately when the bumper is physically activated, as well as three emergency (E-stop) buttons to be pressed by users if needed. The AGV is equipped with a GPS (Global Positioning System) receiver (SX-Blue, Anjou, Quebec, Canada). The GPS receiver is used for sensor data positioning and field mapping rather than for navigation purposes.

The AGV carries three non-invasive crop sensors facing to the right side of the vineyard canopy. The Apogee SI-421 infrared radiometer (Apogee Instruments, Inc., Logan, Utah, USA), displayed in Fig. 1 as *canopy temperature sensor*, measures canopy temperature at a rate of 1.8 Hz and uses the SDI-12 protocol. Its field of view (FOV) covers 36°, resulting in a circular FOV of approximately 0.5 m in diameter according to the distance from the sensor to the vegetation. The spectral sensors to measure the Normalized Difference Vegetation Index (NDVI) and the Photochemical Reflectance Index (PRI) come in four different units: NDVI-hemispherical (Ni), NDVI-field stop (Nr), PRI-hemispherical (Pi) and PRI-field stop (Pr) (SRS for NDVI and PRI, METER Group, Inc.,

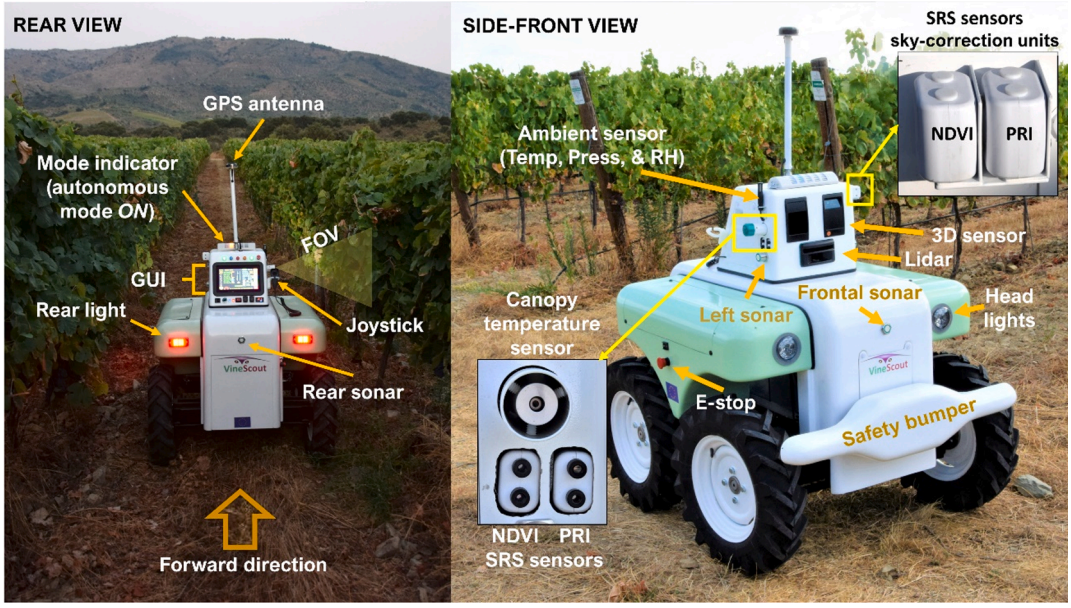

Fig. 1. Main components of the Autonomous Ground Vehicle (AGV) from rear and side-front views. Details of crop sensors and their Field of View (FOV).

Pullman, WA, USA). These units are spectral reflectance sensors (SRS) that measure the electromagnetic radiation reflected from canopy surface after being corrected to current illumination conditions. The NDVI is calculated through bands with a peak wavelength of 650 nm ± 2 nm (with 50 nm full width half maximum, or FWHM) and 810 nm ± 2 nm (with 40 nm FWHM). The PRI bands are centered at 532 nm and 570 nm with 10 nm FWHM. Both SRS sensors have a field of view of 36° (shown as *SRS sensors* in Fig. 1), or a circular diameter of about 0.50 m, and use a hemispherical 180°-FOV Teflon diffuser unit that makes cosine-corrections based on incident irradiation (shown as *SRS sensors – sky-correcting units* in Fig. 1). The sky-correcting units look upwards. Finally, the ambient sensor T7311-2 (COMET SYSTEM, s.r.o., Rožnov pod Radhoštěm, Czech Republic) provides measurements of the local ambient around each vine monitored, in particular, air temperature (°C), atmospheric pressure (hPa), dew temperature (°C), and relative humidity (%). This sensor is shown uncovered in Fig. 1.

2.2. Data collection and field mapping procedure with the AGV

The AGV must be guided with the joystick to the initial position, usually the beginning of the first vineyard row, to start taking data for building the crop map. If GPS performance is at normal levels, the operator turns on the *Data* button of the GUI to start recording all the data set (time, position, ambient, and crop parameters), and then selects the autonomous mode to start moving. The AGV moves along the center line every other row. The GPS antenna is located in the center of the AGV (Fig. 1), getting the coordinates of the trajectory followed by the robot. However, the map-building software also calculates the coordinates of the canopy section at which the crop sensors are pointing at (Rovira-Más et al., 2021), with the intention of having the crop parameters perfectly associated to their actual coordinates in the field (Fig. 2a). In fact, when the AGV detects that there is no vegetation to sense according to the ultrasonic sensor, crop data is not recorded as, for example, during the headland turns or when there are gaps without vegetation within a row. When the map is complete, the operators retrieve the data with a pen-drive through one of the USB ports of the AGV. Field data are saved as ASCII text files (.txt format) and shapefile format (.shp).

The mapping technique to represent field variables follows a global-referenced grid approach (Rovira-Más, 2012). Geodetic coordinates are not suitable for precise operations in agriculture fields. As crop fields can be considered *small* and *flat* compared to the Earth, the representation of crop maps with a Local Tangent Plane (LTP) coordinate system facilitates repeatability during a season and compatibility over the years (Rovira-Más and Sáiz-Rubio, 2013). The LTP coordinate system uses Euclidean geometry, allowing the representation of maps in Cartesian axes with north, east, altitude, and distances expressed in meters. In addition, the LTP coordinate system allows end-users and owners choose a convenient local origin within the field being mapped, so that

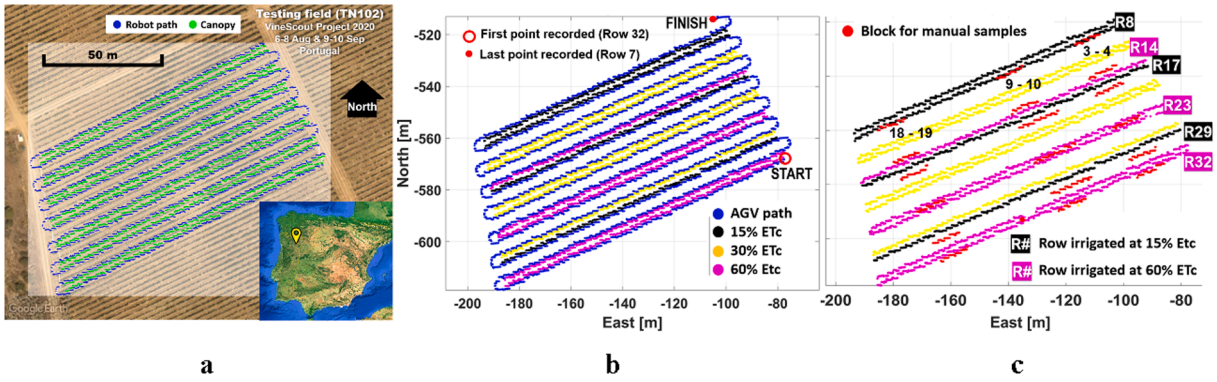

Fig. 2. AGV path and vineyard rows of the testing site (a); Irrigation rates of the rows monitored by the AGV (b); and vineyard blocks for ground-truthing with the rows and their irrigation rates (c).

coordinates always result in manageable numbers. This representation can produce maps of regular square cells after a transformation from LTP coordinates to global grid cells. The size of the cell side can also be chosen by the user to further customize maps. In the present work, the chosen size of the cell side was 2 m, so that rows spaced 2 m apart could be differentiated. This differentiation of the rows was important for the application of specific irrigation rates as one of the key variables to manage in the experiments. The complete process to create global grid maps is described in further detail by Saiz-Rubio and Rovira-Más (2013).

2.3. Data collection with a hand-held pressure chamber for ground-truth validation

Leaf water potential (Ψ_{leaf}) is assumed to represent the mean soil water potential around plant roots, and it is a good indicator of the leaf water status (Ihuoma and Madramootoo, 2017). For this reason, the leaf water potential was used for ground truth validation of the actual hydric status of vine leaves, as it can give satisfying results for assessing vine water status in spite of its physically-demanding practical disadvantages (Rienth and Scholasch, 2019). Leaf water potential was determined using a *Scholander* pressure chamber (Model 600, PMS Instrument Company, Albany, OR, USA). The mode of operation with a pressure chamber started with taking a leaf, then cutting a portion of its petiole with a cutter, and placing it inside the sealed chamber. Pressurized air is slowly released at constant rate into the chamber. As the pressure increases onto the leaf, the xylem sap is forced out until a drop becomes visible at the cut end of the petiole. The pressure applied until the appearance of the drop is equal and opposite to the water potential of the sample (Rienth and Scholasch, 2019).

The testing field (Fig. 2a) had grower-induced hydric status variability achieved with a differential drip irrigation system. In *sustained deficit irrigation,* growers irrigate at a fraction of full crop evapotranspiration (ET_c) throughout the growing season, which is a useful way to save water while maximizing production (Williams, 2010). In order to induce water status variability in the vines, different water regimes were applied to several rows. The irrigation planning was managed according to leaf water potential measurements carried out regularly by the winery technicians. The actual irrigation rates applied are displayed in Table 1. Three different water regimes were established in six rows with two replicates for each water regime. Fig. 2b shows the three different treatments given to the vines: a 60% of the crop evapotranspiration (ET_c), a 30% of the ET_c, and a 15% of the ET_c, and Fig. 2c displays the water regimes and blocks considered in this study. Climate data and reference evapotranspiration (ET_0) was estimated from weather parameters recorded at a meteorological station located nearby, and from the Penman-Monteith equation according to the Food and Agriculture Organization (FAO) (Fernández-Novales et al., 2021). The ET_c is calculated multiplying the ET_0, which is the reference evapotranspiration, by the specific coefficient of the crop (K_c).

2.4. Experimental design and testing vineyard

Although field testing has been ongoing from 2017, the definitive eleven experiments with the last version of the robot featuring the complete crop sensor suite took place in the summer of 2020. The reference plot is located in the Douro Superior sub-region, in a vineyard of the Symington Family Estates winery (Quinta do Ataíde, Portugal) at latitude 41° 14′ 41.4″ N and longitude 7° 06′ 52.9″ W. The seven-year-old *Vitis vinifera* L. cv. Touriga Nacional grafted on 196–17 rootstocks is trained in a vertical shoot position system (VSP), and pruned in Royat single cordon, with a row spacing of 2.20 m and 1 m between plants in the same row. The soil is schistic and predominantly acidic. The manual measurements of water potential with the pressure chamber involved six vineyard rows with two different irrigation treatments (Fig. 2c): three rows irrigated with 15% of the ET_c, and the other three rows irrigated with 60% ET_c, applied according to Table 1. Six blocks per row were selected based on vine vigor roughly defined by the NDVI distribution of the plot from aerial images acquired in a yearly basis. Each block of 5 m comprised five vines. Of these, two sunlit mature representative leaves per vine at medium canopy height were selected to measure the leaf water potential using the Scholander pressure chamber. Overall, a total of 36 blocks were monitored in two periods of the day: morning and midday. Fig. 2c shows the blocks of vines in black numbers (blocks 3 and 4, blocks 9 and 10, block 18 and 19), while rows are displayed in white with a background color depending on the irrigation rate of the row.

Fig. 2a displays the path followed by the AGV over a satellite map of the testing vineyard (Google Earth Pro, Google LLC, Mountain View, CA, USA). The starting position of the robot-generated map was at coordinates E = -77 m and N = -578 m from the user-defined local origin (Fig. 2b). This local origin was placed in a neighboring testing field located north-northeast of the represented map; that is why the coordinates in the Cartesian axes appear negative. The AGV is designed to monitor the right canopy side every two rows, which made the AGV monitor four rows irrigated at 15% ET_c, five rows irrigated at 30% ET_c, and five rows irrigated at 60% ET_c (Fig. 2b). The average velocity of the AGV during field mapping was 1.5 km/h, with an average sampling rate of 0.6 Hz to record time, position, ambient, and crop parameters.

Table 2 summarizes the main characteristics of the eleven field experiments conducted in 2020, whose data were taken on 7th and 8th of August, and on 9th and 10th of September, alternating the mapping time among predawn, morning, midday, or night. However, the nocturnal and part of the predawn tests occurred without the natural illumination that spectral reflectance sensors (NDVI and PRI) required, resulting less informative than the maps acquired during the day, either in the morning or at midday. Along each test identifier, Table 2 indicates the number of valid (filtering outliers) data retrieved for each test, the date when the test was done, the period of the day at which the test took place, and the UTC time (Coordinated Universal Time) at which the experiment registered the first and the last datum. The local time in Portugal was one hour ahead the UTC time. The AGV carried out two kind of tests: the 'block', and the 'map', as shown in the fifth column of Table 2. The type of test named 'map' was configured for the robot to start saving data in the first row continuously until reaching the last vine of the last row. According to the location of the crop sensors in the AGV facing the right side of the vine row, and its forward direction indicating the robot heading, the sensed rows for the tests involving the full map were: 32 (first monitored row, Fig. 2b), 31, 28, 27, 24, 23, 20, 19, 16, 15, 12, 11, 8, and 7 (last monitored row, Fig. 2b). The type of tests classified as 'block' in Table 2, refers to data taken by the AGV only in the spaces, or blocks, marked in red in Fig. 2c, following a stop-and-go procedure. For such tests, each block was delimited by metal posts in the vineyard, and clearly labelled with numbers to facilitate field testing and avoid sampling mistakes. The AGV was positioned at the beginning of each block, and the data recorded along the canopy section were those comprised within the labelled posts. For the blocks of rows 32, 29, 23, 17, 14, and 8, leaf samples were picked from the canopy for the manual measurements with the pressure chamber, assuring the necessary ground truth validation for the model-based predictions of vine water status. The set of data from tests T1, T2, T3, T4, T5, T6, and T8 is published in (Saiz-Rubio et al., 2021), and contains the following columns: Hour (Spanish summer time. The UTC is that value minus 2 h), Minutes, Seconds, Latitude, and Longitude of the AGV antenna, East, and North of the AGV antenna, East, and North of the crop, Altitude, Canopy temperature, Ambient temperature, Pressure, Humidity,

Table 1
Irrigation rates (15% and 60%) applied in the monitored rows for the studied field.

Regime	[1]ET_0 Aug	ET_0 Sept	[2]K_c	Rate Aug	Rate Sept
	mm	mm		(L/ha per week)	(L/ha per week)
15%	27	19	0.7	48,000	32,000
60%	106	75	0.7	184,000	131,000

[1] ET_0: reference evapotranspiration; [2] Kc: crop coefficient.

Table 2
Characteristics of the field experiments with the AGV in 2020 season.

Test name	AGV data points	Manual data points	Date (in 2020)	Period	Start – End (UTC time)	Type	Ground-Truth
T1	1 556	36	7 Aug	Morning	8:25 – 10:10	block	Yes
T2	1 557	36	7 Aug	Midday	12:32 – 16:00	block	Yes
T3	9 533	12	9 Sep	Morning	9:03 – 10:29	map	Yes
T4	9 484	12	9 Sep	Midday	12:29 – 13:40	map	Yes
T5	8 989	12	10 Sep	Morning 1	8:27 – 9:48	map	Yes
T6	11 135	–	8 Aug	Midday	10:44 – 12:14	map	No
T7	10 914	–	10 Sep	Morning 2	10:04 – 11:32	map	No
T8	10 199	–	10 Sep	Midday	11:57 – 13:13	map	No
T9	4 053	–	9 Sep	Predawn	5:26 – 7:49	map	No
T10	2 259	–	8 Aug	Night	21:59 – 23:27	map	No
T11	3 643	–	8 Aug	Predawn	4:40 – 6:11	map	No

Compass heading (direction), NDVI, PRI (averaged), Row, Irrigation rate, Space, and Scholander pressure when it was measured.

Fig. 3 displays the block diagram for the overall data process. The data files saved in the AGV as text files sort information in various columns representing time, position, navigation, climatic conditions, and canopy-related parameters. The parameters relevant for this study provided the test timing, robot position, site-specific ambient conditions, leaf temperature, and vegetative indices. Specifically, the robot *position* comprises three kind of coordinates: the geodetic coordinates directly retrieved from the GPS receiver as latitude (sexagesimal degrees), longitude (sexagesimal degrees), and altitude (meters); the north (meters), east (meters), and altitude (meters) LTP coordinates of the AGV; and the north (m), east (m), and altitude coordinates of the crop canopy. Crop coordinates are the ones used for building crop maps. The ambient parameters monitored with the robot were the following: air temperature (°C), barometric pressure (hPa), and relative humidity (%). The crop parameters include the canopy temperature (°C), the NDVI, and the PRI, being both vegetative indices dimensionless in the range −1 to 1. The data automatically recorded by the AGV was filtered to remove outliers, keeping NDVI values higher than 0 and below 1 to circumvent saturation, or maintaining PRI estimates between −1 and 1. The ground-truth data mentioned in Fig. 3 refers to the leaf water potential (Ψ_{leaf}) manually measured with the pressure chamber, initially output by the chamber's manometer as pressure in bar and transformed here for standardization purposes to MPa. These manual data were collected by experienced technicians, and therefore are considered reliable without the need of further conditioning. Each manual measurement was precisely associated to crop coordinates, such that manual and automatic data were comparable. All the data, both manually and automatically gathered, were conveniently represented over grid maps featuring the same configuration, which facilitated the comparison and statistical correlation among them. This compatibility was guaranteed, in particular, with a common size of the grid maps covering the total area of the testing field, and always maintaining cells with an area of 4 m^2 (2 m × 2 m). Each such square cell contained precise information about air temperature, atmospheric pressure, ambient relative humidity, canopy temperature, NDVI, and PRI. For those cells containing more than one measurement of the same parameter, the average value was considered and plotted. Grid maps are easy to interpret because each cell is assigned a color code according to the range within which the specific value of each parameter falls. Field maps and statistical analyses were carried out with Statgraphics Centurion XVII (Statgraphics Technologies, Inc., The Plains, VA, USA), Matlab (versions R2016b, and R2020a, The MathWorks, Inc., Natick, MA, USA), and Microsoft Excel (version 2016, Microsoft Corporation, Redmond, WA, USA).

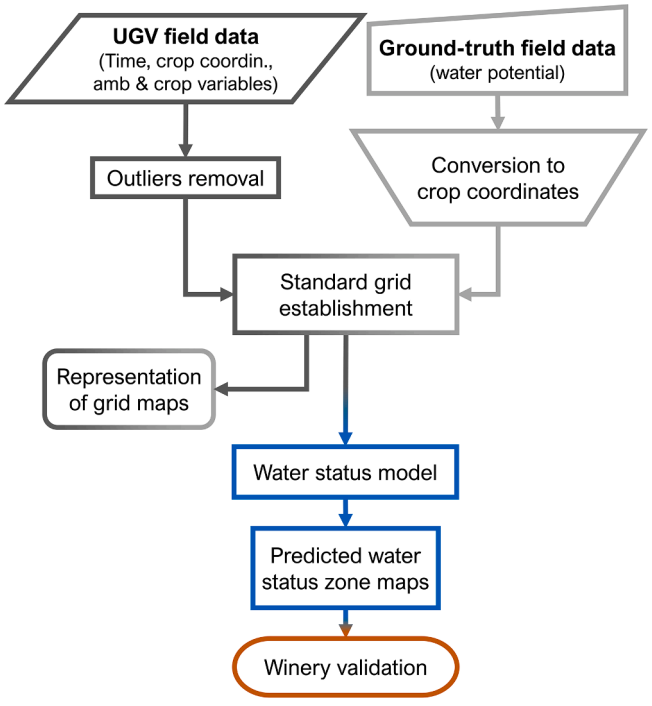

Fig. 3. Field data processing from data collection to representation and evaluation.

To pursue the goal of enouncing a model to automate field measurements and avoid manual data gathering, the suitable tests were those with both ground-truth and robot collected measurements. Thus, the tests used in the statistical analysis were T1 and T2 complete, and from T3, T4, and T5 only the values corresponding to rows 32 and 8 because only sunlit leaves were considered in both manual and automatic tests. The statistical models were computed with multiple regression on the tests T6 to T11. In particular, five models were launched and those with R^2 higher than 58% were evaluated in detail by spatially comparing the water potential predicted with the models and the actual values and ranges. Models with an unnatural distribution of water potential for the experimental conditions tested were discarded. The final water potential model was evaluated and used to determine zones of similar water potential, which were shown to winery technicians for their confirmation and assessment (Fig. 3).

3. Results

Fig. 4 shows the evolution of ambient and crop parameters for the testing vineyard during season 2020. The plot depicts the mean values for each test, which gives an idea of the general variation along August and September. In Fig. 4a, mean ambient and mean canopy temperatures follow the same trend, being the ambient (air) temperature always above canopy temperature. As expected, the lowest temperatures were registered at predawn whereas the maximum temperatures occurred at midday. The ambient temperatures in August were high as a consequence of a heat wave, but not as high as Fig. 4a shows for tests T1 (7th Aug – *mor*), T2 (7th Aug – *mid*), and T6 (8th Aug – *mid*). The reason for that is the lack of a protective cover for the ambient sensor probe as

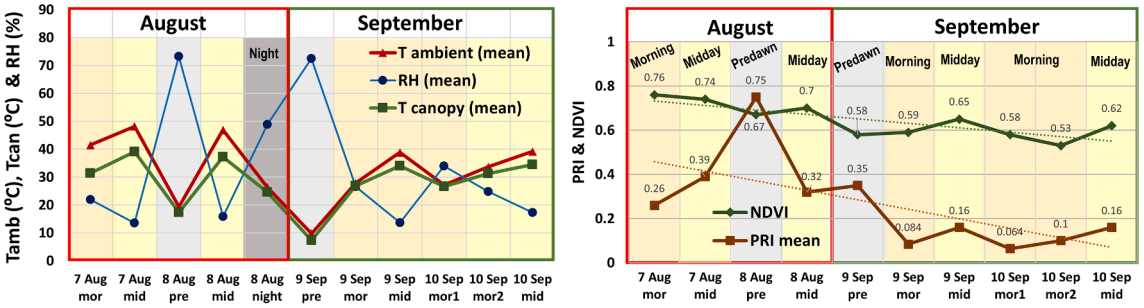

Fig. 4. Mean values for August and September tests (2020): (a) Relative humidity, ambient temperature, and canopy temperature; and (b) PRI and NDVI.

indicated by ISO 17714:2007. Tests in September, however, were done with the probe properly covered from direct sun radiation. Fig. 4a also depicts the mean values of the relative humidity, which show two interesting peaks at predawn coinciding with minimum air temperatures; the contrary is true for midday relative humidity. The lack of illumination in the test that took place at night prevented the use of the passive sensors measuring PRI and NDVI (Fig. 4b), but ambient parameters could be measured (Fig. 4a). Fig. 4b displays the mean values of PRI and NDVI for each test. Mean PRI values were clearly higher in August with an average estimate of 0.43 in comparison to the 0.15 found for September, being higher at midday than in the morning. The same trend is found with the NDVI, which shows a decreasing index along the season with an average NDVI for August of 0.72 in contrast to 0.59 for September.

The model for predicting water potential (MPa), represented by Eq. (1), was obtained after applying multilinear regression to the data sets. The predicted water potential Ψ_{pred}, is a function of six significant field variables: the PRI, the altitude difference ΔAlt (m) as the altitude of each point minus the minimum altitude of the field (153.8 m), the NDVI, the temperature difference (ΔT) between canopy temperature (°C) and ambient temperature (°C), and the relative humidity RH (%). The R^2 for this model was 0.69 (Fig. 5). The data sets used for this model considered the data registered for morning and midday tests in September when the probe of the ambient sensor was properly shielded, but not the data coming from August tests to avoid biasing errors, as the ambient temperature is involved in the model with a considerable weight. Non-linear relationships were also formulated but with inferior results.

$$\Psi_{pred}\ (\text{MPa}) = 0.340 \cdot PRI \ - \ 0.042 \cdot \Delta Alt + 0.017 \cdot NDVI - 0.025 \cdot \Delta T + 0.005 \cdot RH - 1.394 \quad (1)$$

The complete statistical analysis considers the individual correlations among parameters with a higher likelihood of being related from a physiological standpoint. The principal results of these correlations are systematically plotted in Fig. 6, where test timings and irrigation rates are independently marked for each correlation studied. The first correlation analyzed (Fig. 6a) is PRI versus NDVI, with an R^2 of 0.38. In that plot, higher PRI corresponds to August at midday independently of the irrigation rate, followed by PRI values registered in August morning tests, again independently of the irrigation rate. The same occurs for September tests despite having lower PRI average values than August tests (Fig. 4): higher values for midday tests than for morning tests with independency of the irrigation rate. The low R^2 seems related to the disparity in variability distribution; large variations in the NDVI correspond to very strait variations of the PRI. This is clear, for example, for the September 60% morning test, which shows a variation of NDVI of 0.5–0.75 whereas the PRI is contained in the range 0 – 0.1. Fig. 6b plots the PRI versus the temperature difference ΔT, with a consistent coefficient of determination R^2 of 0.75. The representation in Fig. 6b leaves out the test conducted in August at midday to avoid the influence of an overheated probe as a result of a missing shield to prevent direct sun radiation. Unlike Fig. 4 that only considers average values, Fig. 6a yields positive values for the temperature difference, which implies situations and rows with canopy temperatures well above the air temperature. August tests, by contrast, registered ambient temperatures significantly higher than canopy temperatures, leading to negative estimates for ΔT. The six tests (performed in different months and at different time of the day) used to calculate the statistical correlation between the PRI and ΔT evidenced a strong linear dependency between both parameters. Fig. 6c plots canopy temperature versus PRI, and the fact that R^2 is 0.32 indicates that canopy temperature without the ambient correction through the air temperature –in real time– severely reduces the significance of the relationship between both parameters. This finding is important because airborne imagery can track canopy temperature remotely, but real-time corrections with the ambient conditions around the vines are out of reach. As previously observed (Fig. 6a), large variations in canopy temperature are found for similar values of PRI, as for instance, a PRI of 0.25 can be measured for either 28 °C or 37 °C (August 60% morning). In addition, only the morning tests carried out in September showed different canopy temperature according to the irrigation rates, with lower temperature for irrigated rows (60%). In other words, for the extreme heat at midday, irrigation did not make any difference in canopy temperature. Fig. 6d plots canopy temperature versus leaf water potential manually measured with the pressure chamber. With an R^2 of 0.30, this result recalls the output of Fig. 6c; point scattering results in a lack of coherence for most of the tests when comparing with the canopy temperature. Again, the effect of the ambient conditions somehow masks the potential link between water status and leaf temperature. The need of a real-time correction with the air temperature becomes necessary, with the implications for proximal sensing still holding. This was achieved in Fig. 6e for September tests, which plots manually collected water potential versus temperature difference ΔT. The positive effect of correcting canopy temperature with ambient conditions duplicated the R^2 to 0.61, with the meaningful scattering of Fig. 6e. The way the midday test for low irrigated vines (15% ET_c) clusters itself on the negative half (ΔT) of the plot is

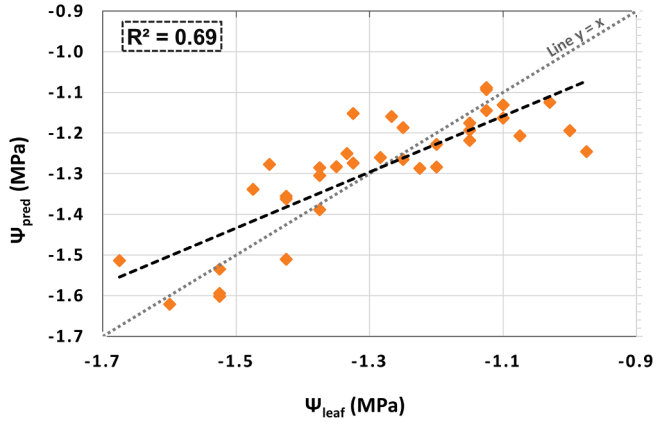

Fig. 5. Water potential model derived from September tests.

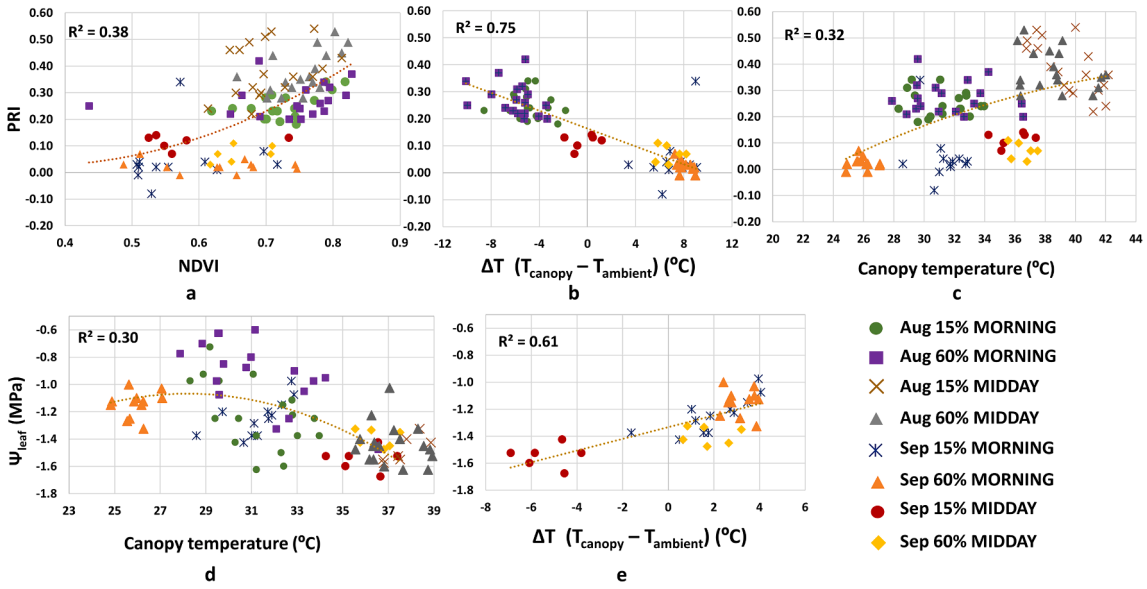

Fig. 6. Individual correlations for season 2020: (a) PRI vs NDVI; (b) PRI vs ΔT; (c) PRI vs canopy temperature; (d) Leaf water potential vs canopy temperature; and (e) Leaf water potential vs ΔT.

remarkable, because the irrigated rows measured at the same time were just in the opposite side of the plot with a positive ΔT. Overall, plants with a higher irrigation rate (60% ET_c) had less negative water potential, which indicates a milder level of plant water stress.

A crucial advantage of grid maps is the convenience of spatially representing variables of interest that result from merging various parameters affecting the same area; for this study in particular, the variable of interest is leaf water potential, which depends on the six variables of the model defined by Eq. (1). Fig. 7a shows the water potential map obtained with Eq. (1) and the field data of test T3, carried out on 9th September from 9 am to 10.30 am (UTC, morning test). The color code simply provides a threshold value of −1.2 MPa to distinguish high and low likelihood of hydric stress. Obviously, such a threshold will normally depend on the moment of the day, as a water potential classified as moderate at midday would probably be severe in the morning. Fig. 7b and Fig. 7c display the NDVI and the altitude grid maps for the testing field, respectively. In all three maps there is a different trend for the center-right region of the field. In the case of the NDVI, it corresponds to high vigor according to the threshold chosen of 0.65; for the altitude, that area corresponds to lower height; and for the water potential, which depends on the two previous maps, it corresponds to a less water stressed zone according to the threshold of −1.2 MPa. Estimated water potential maps for other tests followed a general trend similar to that of Fig. 7a, but with interesting differences due to variations in some of the parameters involved such as the PRI.

Fig. 8 shows the spatial distribution of the PRI along the tests conducted in August and September in the experimental vineyard, together with the alternating irrigation rates and the exposure of each row as sunlit or shaded. In general terms, the PRI always reached higher values in the upper-right section of the field. In test T6, PRI values were positive, whereas zero and negative values erratically appeared during September tests T3 and T4. When comparing outcomes based on day timing for September tests, PRI values were higher for midday than in the morning. Interestingly, for the early morning test T3 (Fig. 8b) the majority of near-zero values correspond to the sunlit side of the rows, but for the midday test T4 (Fig. 8c) many negative PRI values were registered in the shaded side of the rows.

The physical meaning of the PRI is related to the photosynthetic efficiency of the vines' leaves, and therefore it is a complex parameter to interpret. Fig. 8 provides a spatial–temporal analysis of its distribution within the vineyard, but deeper insights underlie in the graph of Fig. 9, where the ordinate axis shows the PRI, ΔT, canopy temperature and ambient temperature, whereas the abscissa axis shows the test timing in minutes. The right axis indicates the moving direction or heading. In particular, the AGV monitored the sunlit side of the canopy when heading was around 250°, and the shaded side when heading was about 60°. The graph also highlights the rows that were sunlit or shaded with a different background color for the rows, and the irrigation rates of 60%, 30%, or 15% of the ET_c. Sunlit canopies kept PRI values near zero or slightly above for these midday conditions; however, the PRI had a wider dispersion for the shaded rows with most values oscillating in the range −1 to 1. Air temperature was steadily growing along the test, which is something expected as the test began at 12:29 UTC and ended at 13:40 UTC (midday test). The highest temperatures in the

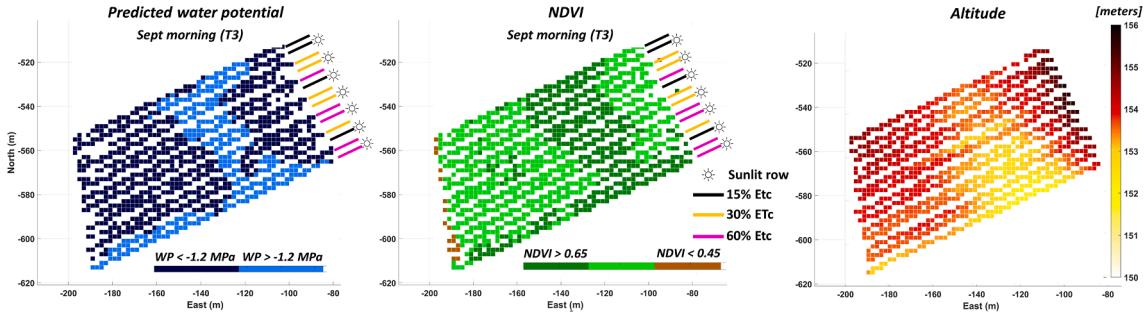

Fig. 7. Grid maps for T3: (a) Estimated water potential (MPa); (b) altitude (m); and (c) NDVI.

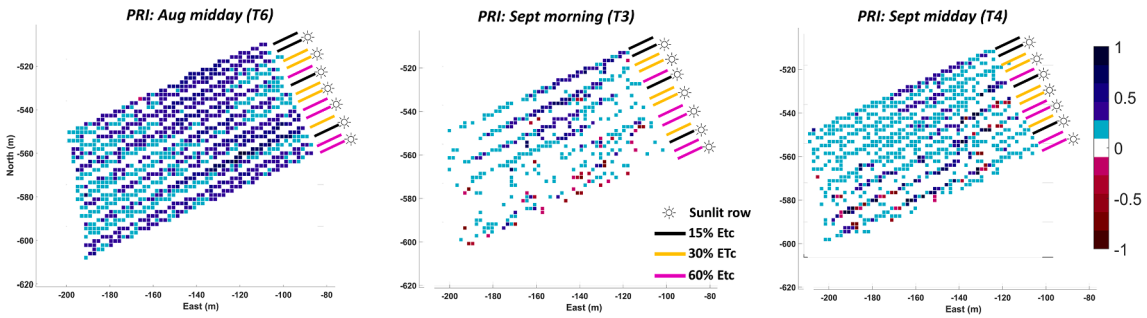

Fig. 8. Maps showing the spatial and temporal variability of PRI: midday in August (a), morning in September (b), and midday in September (c).

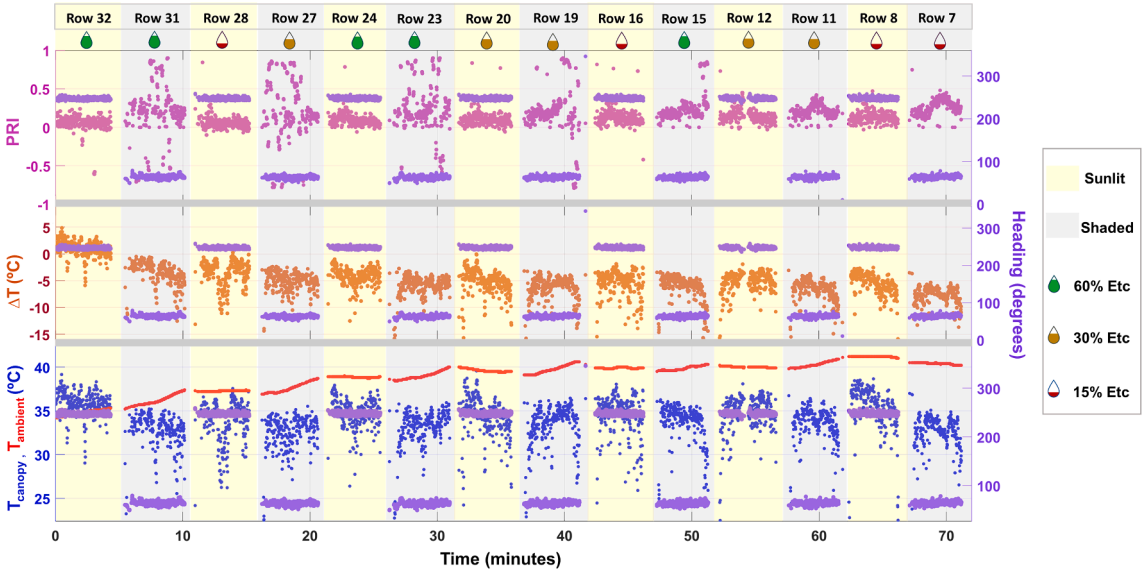

Fig. 9. PRI, ΔT, canopy temperature, and air temperature for test T4 (September at midday).

experimental vineyard have been recorded in the afternoon, around 16:00 UTC. Canopy temperatures, on the contrary, show an oscillating pattern with higher measurements for the sunny side of the canopy, although overall, the canopy temperature remained stable in average. As a result, ΔT was negative for all the rows except for the first, in which it was close to zero. This means that in midday conditions, the air temperature is typically above the canopy temperature, unlike morning conditions.

Table 3 shows the canopy temperature and PRI when comparing sunlit and shaded canopy sides. The difference in canopy temperature between sunlit and shaded leaves reached 1.8° during morning test T3 (September). For midday test T4 (September) when the sun was more vertically aligned, these differences were smaller and reached 1.6°. However, the PRI behaved inversely; higher values were registered for the shaded canopy side with differences up to 0.15.

Table 3
Mean values of canopy temperature and PRI collected with the AGV on sunlit and shaded canopy sides.

Test	Month	Period	Variable	Mean value		Difference
				Sunlit canopy	**Shaded canopy**	**[Sunlit – Shaded]**
T6	August	Midday	Tcanopy	37.65	36.78	0.87
			PRI	0.26	0.37	−0.11
T3	September	Morning	Tcanopy	27.6	25.8	1.8
			PRI	0.01	0.16	−0.15
T4	September	Midday	Tcanopy	34.78	33.15	1.63
			PRI	0.10	0.23	−0.13

The statistical analysis revealed, with a confidence level of 95%, that both manually and predicted water potential produced significant differences for rows irrigated differently, in particular with rates 15% ET_c versus 60% ET_c. The final stage of this research consists of quantifying how close measured and predicted water potential are for the suite of situations studied, and how tests differ among them. Fig. 10 depicts the predicted water potential respect the real values for tests T1 (a), T2 (b), T3 (c), and T4 (d); T3 is plotted in Fig. 7a as a grid map. As manual measurements were conducted at 36 selected points of the experimental vineyard (Fig. 2c), there is no point in drawing a complete grid map of the estimations carried out with the pressure chamber, but the analysis of residuals can be performed through Table 4, and Table 5. The results drawn from those tables indicate that average errors ranged from 0.79 (T5 test, Table 5) to 2.43 (T1 test, Table 4). The mean absolute error, or MAE, has been used to measure prediction accuracy. MAE is the average absolute difference between the predicted value and the actual value at some specific point (Moroney, 2021). Thus, the average error of Table 4 and Table 5 has been calculated as MAE: the sum of the predicted water potential values minus the sum of actual water potential values (Scholander). The result is made positive (taking the absolute value), and then dividing by 36 points for T1 and T2, or by 12 for T3, T4, and T5. Reasonably, the model estimates better the tests performed in September than in August (Fig. 10, Table 5), as the final statistical model was chosen from that conformed by September tests (Fig. 10a,b), but also, the test T2 (Fig. 10b) had a similar low error despite being a test from August (midday). However, the test T1 (Fig. 10a) from August at morning, had higher errors in the estimates. Those estimates are lower than the real Scholander values, which makes sense as the September

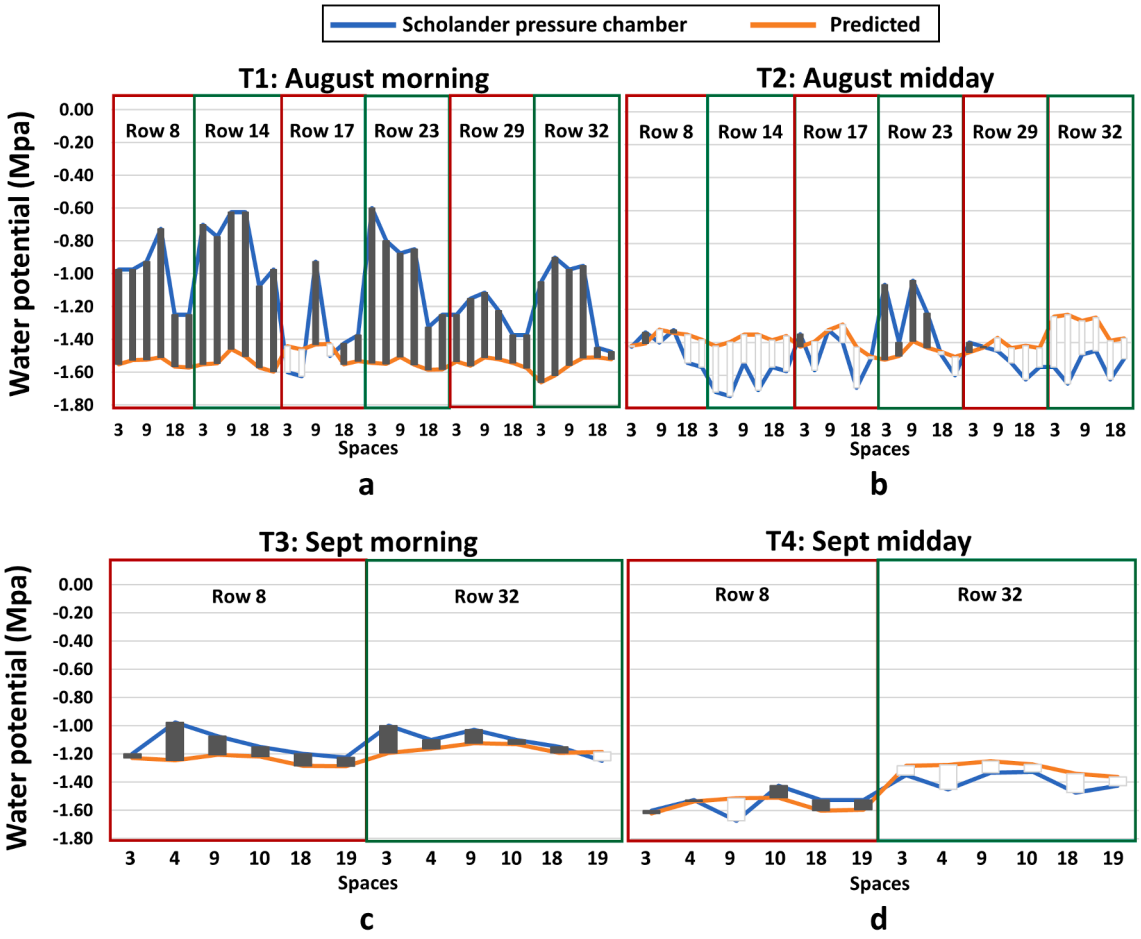

Fig. 10. Measured and predicted water potential values per row in August: T1 (a), and T2 (b) tests, and September: T3 (c), and T4 (d) tests.

values (statistical model) had lower temperatures.

The importance of the analysis of residues, i.e. the difference between predicted and actual values, rests on the fact that it allows to assess how good a model is regardless of the method used to define it. At present, there is a plethora of modelling techniques – Principal Component Analysis (PCA), multivariate analysis, Artificial Intelligence (AI) techniques…- some more complex than others, but the real focus would be on the goodness of the fit and the versatility of the model as many diverse situations as possible.

According to Fig. 3 (block diagram), the ultimate feedback has to be received from the wine maker as the final end-user of the produced grapes. The experimental vineyard (Fig. 2) used in this study is actually a commercial vineyard, which has been the source of two distinct wines. While oenologists do not actually draw a zone map every harvest, they analyzed the grapes coming from these experience-determined zones as well as the properties of the resulting wines. Due to the specific environmental characteristics of 2020, the west section of the vineyard in Fig. 7a allowed for a separate vinification of the grapes. Those vines reached a potential for a higher class wine when compared to the rest of the field, with an economic gain that can reach 85% of the value compared to the base blend.

4. Discussion

This study proposes a methodology and a model, to assess grapevine water status from a set of specific relevant parameters measured non-invasively from an AGV. The representation of variability across selected field parameters and sought hydric state was enhanced with their precise display in grid maps, upon which appeared interesting relationships among parameters; some already mentioned in the state of the art, and some new or overlooked. Although the data feeding the water status model was gathered in 2020, the experimental field has been closely monitored by the AGV since 2017. As a result, the evolution of key parameters along each season has been richly documented, helping to understand how ambient local conditions affect vineyard behavior. Canopy temperature, for instance, is directly influenced by ambient temperature and relative humidity. On-the-go NDVI measurements from the AGV revealed an alternative perspective to monitoring vineyard vigor and health from proximity. Such a high-resolution monitoring also revealed unexpected measurements for midday conditions (Fig. 4b), which point at coupling effects between NDVI spectral measurements including crop-sensor orientation and sun radiation intensity. Unlike the widespread NDVI, the less known PRI was also tracked seasonally with the AGV, with a decreasing trend along the season that coincided with previous studies (Magney et al., 2016). Specifically, mean PRI values were higher in August (0.26–0.39) than in September (0.06–0.16), and they were higher at midday than in the morning, following a trend similar to the canopy temperature. But what made PRI interesting was gaining insights in how reactive it was on a daily basis, as PRI is set to monitor the diurnal photosynthetic regulation of plants, including subtle dynamics arising from alternations in physiological activity (Gamon et al., 2015). The fact that the daily trend of PRI has been reported to yield different results depending on the crop or even on the specie (Merlier et al., 2015) makes its analysis intriguing, taking into account the particular characteristics of the vine variety *Touriga Nacional* used in this research. Furthermore, controversial results have been reported on the PRI differences for sunlit and shaded sides of the canopy. Zhang et al. (2016) for several tree species and Evain

Table 4
Block-by-block analysis of residuals for non-invasive estimation of water potential: tests T1 and T2.

Point	T1			T2		
	Real	Pred	Error	Real	Pred	Error
1	−0.98	−1.55	0.58	−1.43	−1.42	−0.01
2	−0.98	−1.53	0.55	−1.34	−1.41	0.07
3	−0.93	−1.52	0.60	−1.40	−1.32	−0.08
4	−0.73	−1.51	0.78	−1.33	−1.34	0.02
5	−1.25	−1.57	0.32	−1.53	−1.35	−0.17
6	−1.25	−1.57	0.32	−1.55	−1.39	−0.16
7	−0.70	−1.55	0.85	−1.70	−1.42	−0.28
8	−0.78	−1.55	0.77	−1.73	−1.40	−0.33
9	−0.63	−1.46	0.83	−1.53	−1.35	−0.17
10	−0.63	−1.50	0.88	−1.69	−1.35	−0.34
11	−1.08	−1.57	0.50	−1.55	−1.39	−0.16
12	−0.98	−1.60	0.62	−1.58	−1.36	−0.21
13	−1.60	−1.44	−0.16	−1.35	−1.43	0.08
14	−1.63	−1.46	−0.17	−1.57	−1.40	−0.17
15	−0.93	−1.43	0.50	−1.33	−1.32	0.00
16	−1.50	−1.43	−0.07	−1.40	−1.29	−0.11
17	−1.43	−1.55	0.13	−1.68	−1.43	−0.25
18	−1.38	−1.53	0.16	−1.50	−1.49	−0.01
19	−0.60	−1.54	0.94	−1.05	−1.50	0.45
20	−0.80	−1.55	0.75	−1.40	−1.48	0.08
21	−0.88	−1.51	0.63	−1.03	−1.39	0.37
22	−0.85	−1.55	0.70	−1.23	−1.43	0.21
23	−1.33	−1.59	0.26	−1.48	−1.46	−0.02
24	−1.25	−1.58	0.33	−1.60	−1.49	−0.11
25	−1.25	−1.54	0.29	−1.40	−1.46	0.06
26	−1.15	−1.56	0.41	−1.43	−1.43	0.01
27	−1.12	−1.51	0.39	−1.45	−1.37	−0.08
28	−1.23	−1.52	0.30	−1.53	−1.43	−0.09
29	−1.38	−1.54	0.17	−1.63	−1.42	−0.21
30	−1.38	−1.57	0.20	−1.55	−1.44	−0.11
31	−1.05	−1.66	0.61	−1.55	−1.24	−0.31
32	−0.90	−1.62	0.72	−1.65	−1.23	−0.42
33	−0.98	−1.56	0.58	−1.48	−1.27	−0.21
34	−0.95	−1.51	0.56	−1.45	−1.25	−0.20
35	−1.45	−1.51	0.06	−1.63	−1.39	−0.24
36	−1.48	−1.52	0.05	−1.50	−1.38	−0.12
Absolute error			16.72			5.90
MAE (Avg error)			0.46			0.16

et al. (2004) for vineyards, both reported lower PRI values for sunlit leaves than for shaded leaves, which totally coincides with the results of this study as shown in Table 3 or Fig. 9. However, Yang et al., 2019 reported just the opposite for wheat, i. e. lower PRI for the shaded side of the canopy than for the sunlit side. Nevertheless, considering that grapevines have a lignified trunk and behave in a similar trend to other trees when compared to annual crops, it makes sense to corroborate lower PRI estimates for sunlit leaves. While the results of intensive data acquisition for the PRI resulted informative and novel, the mechanisms involved in PRI variation are complex and many physical, biochemical, and physiological factors can affect diurnal and seasonal PRI patterns at foliar, canopy and ecosystemic levels (Zhang et al., 2016), leaving still a long way open for research.

The intense monitoring of multiple field parameters led to multiple relationships among them: some stronger than others, and some more interesting than others. A strong relationship between PRI and canopy temperature was already noticed for airborne techniques in corn, with R^2 of 0.72 (Suárez et al., 2009) and R^2 of 0.82 (Rossini et al., 2013). Interestingly, moving from remote zenithal views to sub-meter side views, and changing large coverage images by sampled canopy areas well below the square meter, led to a completely different scenario. For this study, such relationship resulted in an R^2 of 0.32 (Fig. 6c), which is in line with researchers reporting that plant temperature is linearly related to evapotranspiration and largely influenced by site-specific microclimatic conditions and their changes, such as air temperature, wind speed, or radiation intensity (Maes and Steppe, 2012; Poirier-Pocovi and Bailey, 2020). It is important to keep in mind that the present research brings novelty in two aspects: crop proximity and massive sampling, and consistency with prior results under diverse conditions implies a solid step forward for understanding plant physiological responses. When the real-time difference between air and canopy temperatures was defined as a key modeling parameter instead of just the canopy temperature, its correlation with the PRI improved significantly up to an R^2 of 0.75 (Fig. 6b). The advantages of using this temperature difference for assessing water status had been already reported for airborne images of corn (Rossini et al., 2013), and for field-fixed sensors in squash, alfalfa, and soybeans (Idso et al., 1981). As a matter of fact, Testi et al. (2008) claimed that taking the difference of temperatures makes sense because that normalization can unlink physiological effects on the canopy heat balance from the physical effects of radiation, convection, and vapor pressure. But yet more interesting for automated water stress assessment is the strong correlation found between leaf water potential and temperature difference, with an R^2 of 0.61 as plotted in Fig. 6e, and the lack of a stronger correlation with water potential when air temperature is not considered, with a weak R^2 of 0.30 (Fig. 6d). In the same line of thought, Ehrler et al. (1978) stated that if canopy temperature could respond to changes in plant water potential, and therefore, be used for long term crop monitoring, the temperature difference was better for sensing plant response to drought. In addition to the temperature difference, other variables included in the water potential model proposed in this study (Eq. (1), Fig. 5) have been reported to respond to water potential as well; in particular, the PRI (Evain et al., 2004; Ihuoma & Madramootoo, 2017; Suárez et al., 2008; Thenot et al., 2002) and the NDVI (Ihuoma and Madramootoo, 2017), which not only responded to the natural growth rate of plants, but also to the changes

Table 5
Block-by-block analysis of residuals for non-invasive estimation of water potential: tests T3, T4 and T5.

Point	T3			T4			T5		
	Real	Pred	Error	Real	Pred	Error	Real	Pred	Error
1	−1.20	−1.23	0.03	−1.60	−1.62	0.02	−1.38	−1.39	0.01
2	−0.98	−1.25	0.27	−1.53	−1.53	0.01	−1.43	−1.36	−0.07
3	−1.08	−1.21	0.13	−1.68	−1.51	−0.16	−1.28	−1.26	−0.02
4	−1.15	−1.22	0.07	−1.43	−1.51	0.09	−1.25	−1.27	0.02
5	−1.20	−1.28	0.08	−1.53	−1.60	0.08	−1.38	−1.28	−0.09
6	−1.23	−1.29	0.06	−1.53	−1.59	0.07	−1.38	−1.30	−0.07
7	−1.00	−1.19	0.19	−1.35	−1.28	−0.07	−1.15	−1.18	0.03
8	−1.10	−1.16	0.06	−1.45	−1.28	−0.17	−1.13	−1.14	0.02
9	−1.03	−1.12	0.09	−1.33	−1.25	−0.08	−1.13	−1.09	−0.04
10	−1.10	−1.13	0.03	−1.33	−1.27	−0.05	−1.13	−1.09	−0.03
11	−1.15	−1.19	0.04	−1.48	−1.34	−0.14	−1.33	−1.15	−0.17
12	−1.25	−1.19	−0.06	−1.43	−1.36	−0.06	−1.27	−1.16	−0.11
Absolute error		1.13			1.00			0.68	
MAE (Avg error)		0.09			0.08			0.06	

originated by introducing different irrigation rates in the experimental setup of this research. In fact, the NDVI has been linearly related to canopy growth (Trout et al., 2008), and canopy growth has been shown to be a key factor determining grapevine water use (Williams and Ayars, 2005).

The value of the present analysis rests on the power of field data understood as the right balance between quantity and quality. In that respect, the suite of sensors selected for this research resulted advantageous for the non-invasive monitoring of water status in grapevines from an AGV. The benefits of using infrared radiometers for recording canopy temperature, as a nondestructive and cost-effective technology that can be mounted on mobile platforms, has been proved to detect differences between sunlit and shaded canopy sides (King et al., 2021), showing that sunlit leaves were significantly warmer in confirmation of Table 3 and in agreement with Van Zyl (1986). The real-time combination of the infrared radiometer, the PRI sensor, and the NDVI sensor with the ambient sensor providing air temperature and relative humidity, greatly improved the estimation of water potential and facilitated the graphical representation of its spatial distribution over the vineyard. The maps displayed in Fig. 7 reproduce recognizable features of the monitored vineyard based on grower's records. The NDVI map, in particular, resembles to the airborne-based NDVI map delivered by a service company hired by the owner in a yearly basis. However, a parameter that will need a further analysis is the altitude difference. It improved the water potential prediction model in this research as it is highly related to the water readily available for the plant in fields with noticeable differences in altitude, but special caution is needed when interpreting the weight of this parameter in future models as the altitude difference presents a non-linear behavior, and therefore more diverse, and larger data sets are needed for a deeper statistical study.

Several outcomes from this study invite to search deeper in the parameters recorded by the AGV. The contribution of PRI to water stress detection, for example, is affected by canopy structure, cover, and viewing geometry (Panigada et al., 2014; Rossini et al., 2013), and although Thenot et al. (2002) demonstrated the sensitivity of PRI to water stress conditions, the effects of stress on the canopy structure may also affect the reflectance signal, something that needs to be further studied. Other parameters, in addition, also present important challenges that need being addressed before their integration in water potential models, as water stress can affect the characteristics of the fruits and the future wine both positively and negatively. Despite the fact that Alves et al. (2013, 2012) reported that non-irrigated grapevines experienced severe water stress and consequently lower photosynthetic rates, many vines that are water stressed have been found to bear fruit with a higher concentration of sugar than vines that are given more water (Williams, 2010). By contrast, moderate levels of irrigation have a positive impact on leaf gas exchange rates, and on yield and berry quality (Alves et al., 2013). As the potential quality of wines has been shown to be affected by water stress, the precise estimation of water potential to set optimal irrigation rates will be crucial for producing premier wines. For the experiments conducted in the testing vineyard, leaf water potential –both manually collected with the pressure chamber and predicted with the robot– showed significant differences for rows differently irrigated at 15% ET_c and at 60% ET_c.

5. Conclusions

The automation of data recording with AGVs (Autonomous Ground Vehicles) resulted instrumental to characterize a vineyard with massive data. This characterization led to confirm some general trends while finding new relationships between vegetative indices, crop features, and ambient conditions. In this line, the correlation between temperature difference ΔT and PRI with an R^2 of 0.75, and between ΔT and ground-truth leaf water potential with an R^2 of 0.61, both indicate the capacity of real-time non-invasive sensing to extract relevant physiological information from the plants. The particular combination of canopy-air temperature difference ΔT with spectral indices PRI and NDVI provided good prospects for defining a novel model capable of tracking water potential non-invasively and from moving platforms, with a coefficient of determination R^2 of 0.69. However, the model was fit with data acquired in September and in a particular region. A natural extension of this work will necessarily try to make the model more robust with data from diverse regions, altitudes, and latitudes. The representation of large amounts of data coming from multiple field tests was possible thanks to the rationalization of measurements in grid-based maps while maintaining global references with the local tangent plane (LTP) coordinate system. Not only visualization was enhanced but also the correlation among parameters was facilitated. In the end, the high-resolution maps of water potential developed in this work have multiple destinations for end-users: first, the spatial variations of vine hydric state provide truthful information at the time of deciding a dynamic irrigation schedule; second, to define differentiated harvesting zones, as wine quality greatly improves when grapes of diverse properties are not mixed, and the relationship between hydric stress and grape quality has been previously proved; and third, serving as a complement for airborne data or anonymized large-scale data handled by other public or private institutions. In addition to stimulate delving into the spectral indices NDVI, PRI, and other ones bringing complementarity, this research may encourage the acquisition of massive data from crops with autonomous ground vehicles, as a facilitator and forerunner for the further application of sophisticated artificial intelligence (AI) algorithms that help growers better understand how plants grow and produce fruit under a changing and unpredictable environment.

CRediT authorship contribution statement

Verónica Saiz-Rubio: Software, Formal analysis, Data curation, Investigation, Methodology, Project administration, Writing – original draft, Writing – review & editing. **Francisco Rovira-Más:** Conceptualization, Software, Data curation, Formal analysis, Investigation, Methodology, Project administration, Supervision, Writing – review & editing. **Andrés Cuenca-Cuenca:** Methodology, Software, Investigation. **Fernando Alves:** Validation, Investigation, Resources.

Declaration of Competing Interest

The authors declare that they have no known competing financial interests or personal relationships that could have appeared to influence the work reported in this paper.

Acknowledgements

This work has been developed under grant agreement N°737669 of the European Union's Horizon 2020 research and innovation program, and it has received the support of Symington Family States owners and technicians, whose assistance is deeply appreciated. In particular, the Symington family (Dominic, John, and Charles), and staff members Joana Valente, Artur Moreira, and Pedro Leal da Costa. Likewise, Juan José Peña Suárez and Montano Pérez Teruel from the Universitat Politècnica de València in Spain are greatly thanked for their continuous support.

Funding: This work was supported by the European Union's Horizon 2020 research and innovation programme (grant agreement number 737669). The opinions expressed reflect only the authors' view. Neither the European Commission, nor the funding agency, nor its services are responsible for any use that may be made of the information that this publication contains.

References

Alves, F., Costa, J., Costa, P., Correia, C., Gonçalves, B., Soares, R., Moutinho-Pereira, J., 2012. Influence of climate and deficit irrigation on grapevine physiology, yield and

quality attributes, of the cv. TourigaNacional at Douro Region, in: IXe International Terroirs Congress. Dijon-Reims, France, p. Vol. 2, Session 7: 20-24.
Alves, F., Costa, J., Costa, P., Correria, C., Gonçalves, B., Soares, R., Moutinho-Pereira, J., 2013. Grapevine water stress management in douro region: long term physiology, yield and quality studies in cv. Touriga Nacional, in: 18th International Symposium GiESCO.
Cohen, Y., Alchanatis, V., Meron, M., Saranga, Y., Tsipris, J., 2005. Estimation of leaf water potential by thermal imagery and spatial analysis. J. Exp. Bot. 56, 1843–1852. https://doi.org/10.1093/jxb/eri174.
Della Cava, M., 2019. Climate change is coming for your wine. What the world's wineries are doing to save grapes [WWW Document]. USA Today. URL https://eu.usatoday.com/story/news/nation/2019/09/08/climate-change-threatens-worlds-wineries-which-grapes-saved/2136457001/ (accessed 11.10.20).
Ehrler, W.L., Idso, S.B., Jackson, R.D., Reginato, R.J., 1978. Wheat Canopy Temperature: Relation to Plant Water Potential 1. Agron. J. 70, 251–256. https://doi.org/10.2134/agronj1978.00021962007000020010x.
Evain, S., Flexas, J., Moya, I., 2004. A new instrument for passive remote sensing: 2. Measurement of leaf and canopy reflectance changes at 531 nm and their relationship with photosynthesis and chlorophyll fluorescence. Remote Sens. Environ. 91, 175–185. https://doi.org/10.1016/j.rse.2004.03.012.
Fernández-Novales, J., Saiz-Rubio, V., Barrio, I., Rovira-Más, F., Cuenca-Cuenca, A., Alves, F., Valente, J., Tardáguila, J., Diago, M.P., 2021. Monitoring and mapping vineyard water status using non-invasive technologies by a ground robot. Biosyst. Eng. Submitted for publication.
Fernandez Esteban, C., 2019. El cambio climático redibujará el mapa de viñedos en todo el mundo [WWW Document]. Bus. Insid, España https://www.businessinsider.es/cambio-climatico-redibujara-mapa-vinedos-todo-mundo-540379 (accessed 11.10.20).
Fountas, S., Mylonas, N., Malounas, I., Rodias, E., Hellmann Santos, C., Pekkeriet, E., 2020. Agricultural Robotics for Field Operations. Sensors 20, 2672. https://doi.org/10.3390/s20092672.
Fraga, H., de Cortázar, García, Atauri, I., Malheiro, A.C., Moutinho-Pereira, J., Santos, J. A., 2017. Viticulture in Portugal: A review of recent trends and climate change projections. OENO One 51, 61. https://doi.org/10.20870/oeno-one.2016.0.0.1621.
Gamon, J.A., Kovalchuck, O., Wong, C.Y.S., Harris, A., Garrity, S.R., 2015. Monitoring seasonal and diurnal changes in photosynthetic pigments with automated PRI and NDVI sensors. Biogeosciences 12, 4149–4159. https://doi.org/10.5194/bg-12-4149-2015.
Gamon, J.A., Serrano, L., Surfus, J.S., 1997. The photochemical reflectance index: an optical indicator of photosynthetic radiation use efficiency across species, functional types, and nutrient levels. Oecologia 112, 492–501.
González-Flor, C., Serrano, L., Gorchs, G., 2019. Use of reflectance indices to assess vine water status under mild to moderate water deficits. Agronomy 9, 1–16. https://doi.org/10.3390/agronomy9070346.
Guisard, Y., 2009. Crop canopy temperature as indicator of water stress: Application to grapevines. Charles Sturt University.
Idso, S.B., Jackson, R.D., Pinter, P.J., Reginato, R.J., Hatfield, J.L., 1981. Normalizing the stress-degree-day parameter for environmental variability. Agric. Meteorol. 24, 45–55. https://doi.org/10.1016/0002-1571(81)90032-7.
Ihuoma, S.O., Madramootoo, C.A., 2017. Recent advances in crop water stress detection. Comput. Electron. Agric. 141, 267–275. https://doi.org/10.1016/j.compag.2017.07.026.
Intrigliolo, D.S., Castel, J.R., Cárcel, S., 2008. Effects of crop level and irrigation on yield and wine quality of tempranillo grapevines in a dry year. In: Acta Horticulturae. International Society for Horticultural Science, pp. 371–378.
Jones, G.V., Alves, F., 2012. Impact of climate change on wine production: a global overview and regional assessment in the Douro Valley of Portugal. Int. J. Glob. Warm. 4, 383–406.
King, B.A., Tarkalson, D.D., Sharma, V., Bjorneberg, D.L., 2021. Thermal Crop Water Stress Index Base Line Temperatures for Sugarbeet in Arid Western U.S. Agric. Water Manage. 243, 106459. https://doi.org/10.1016/j.agwat.2020.106459.
Maes, W.H., Steppe, K., 2012. Estimating evapotranspiration and drought stress with ground-based thermal remote sensing in agriculture: a review. J. Exp. Bot. 63, 4671–4712.
Magney, T.S., Vierling, L.A., Eitel, J.U.H., Huggins, D.R., Garrity, S.R., 2016. Response of high frequency Photochemical Reflectance Index (PRI) measurements to environmental conditions in wheat. Remote Sens. Environ. 173, 84–97. https://doi.org/10.1016/j.rse.2015.11.013.
Merlier, E., Hmimina, G., Dufrêne, E., Soudani, K., 2015. Explaining the variability of the photochemical reflectance index (PRI) at the canopy-scale: Disentangling the effects of phenological and physiological changes. J. Photochem. Photobiol. B Biol. 151, 161–171. https://doi.org/10.1016/j.jphotobiol.2015.08.006.
Moroney, L., 2021. AI and Machine Learning for Coders: A Programmer's Guide to Artificial Intelligence. O'Reilly Media Inc., Sebastopol, CA.
Ortuani, Facchi, Mayer, Bianchi, Bianchi, Brancadoro, 2019. Assessing the Effectiveness of Variable-Rate Drip Irrigation on Water Use Efficiency in a Vineyard in Northern Italy. Water 11, 1964. https://doi.org/10.3390/w11101964.
Panigada, C., Rossini, M., Meroni, M., Cilia, C., Busetto, L., Amaducci, S., Boschetti, M., Cogliati, S., Picchi, V., Pinto, F., Marchesi, A., Colombo, R., 2014. Fluorescence, PRI and canopy temperature for water stress detection in cereal crops. Int. J. Appl. Earth Obs. Geoinf. 30, 167–178. https://doi.org/10.1016/j.jag.2014.02.002.
Pôças, I., Gonçalves, J., Costa, P.M., Gonçalves, I., Pereira, L.S., Cunha, M., 2017. Hyperspectral-based predictive modelling of grapevine water status in the Portuguese Douro wine region. Int. J. Appl. Earth Obs. Geoinf. 58, 177–190. https://doi.org/10.1016/j.jag.2017.02.013.
Poirier-Pocovi, M., Bailey, B.N., 2020. Sensitivity analysis of four crop water stress indices to ambient environmental conditions and stomatal conductance. Sci. Hortic. Amsterdam). 259, 108825.
Rienth, M., Scholasch, T., 2019. State-of-the-art of tools and methods to assess vine water status. Oeno One 53, 619–637. https://doi.org/10.20870/oeno-one.2019.53.4.2403.
Rossini, M., Fava, F., Cogliati, S., Meroni, M., Marchesi, A., Panigada, C., Giardino, C., Busetto, L., Migliavacca, M., Amaducci, S., Colombo, R., 2013. Assessing canopy PRI from airborne imagery to map water stress in maize. ISPRS J. Photogramm. Remote Sens. 86, 168–177. https://doi.org/10.1016/j.isprsjprs.2013.10.002.
Rovira-Más, F., 2012. Global-referenced navigation grids for off-road vehicles and environments. Rob. Auton. Syst. 60, 278–287. https://doi.org/10.1016/j.robot.2011.11.007.
Rovira-Más, F., Sáiz-Rubio, V., 2013. Crop biometric maps: The key to prediction. Sensors (Switzerland) 13, 12698–12743. https://doi.org/10.3390/s130912698.
Rovira-Más, F., Saiz-Rubio, V., Cuenca-Cuenca, A., 2021. Sensing architecture for terrestrial crop monitoring: harvesting data as an asset. Sensors Submitted.
Rovira-Más, F., Saiz-Rubio, V., Cuenca-Cuenca, A., 2020. Augmented Perception for Agricultural Robots Navigation. IEEE Sens. J. 1–1 https://doi.org/10.1109/jsen.2020.3016081.
Saiz-Rubio, V., Rovira-Más, F., 2020. From Smart Farming towards Agriculture 5.0: A Review on Crop Data Management. Agronomy 10, 207. https://doi.org/10.3390/agronomy10020207.
Saiz-Rubio, V., Rovira-Más, F., 2013. Proximal sensing mapping method to generate field maps in vineyards. Agric. Eng. Int. CIGR J. 15, 47.
Saiz-Rubio, V., Rovira-Más, F., Broseta-Sancho, P., Aguilera-Hernández, R.A., 2015. Robot-generated crop maps for decision-making in vineyards, in: American Society of Agricultural and Biological Engineers Annual International Meeting 2015. St. Joseph, Mich.: ASABE, New Orleans, Louisiana, USA, pp. 4097–4104. https://doi.org/10.13031/aim.20152189909.
Saiz-Rubio, V., Rovira-Más, F., Cuenca-Cuenca, A., 2021. VineScout EU project - Summer 2020 data. https://doi.org/10.5281/zenodo.4432057.
Santesteban, L.G., Miranda, C., Royo, J.B., 2011. Suitability of pre-dawn and stem water potential as indicators of vineyard water status in cv. Tempranillo. Aust. J. Grape Wine Res. 17, 43–51. https://doi.org/10.1111/j.1755-0238.2010.00116.x.
Santos, J.A., Fraga, H., Malheiro, A.C., Moutinho-Pereira, J., Dinis, L.-T., Correia, C., Moriondo, M., Leolini, L., Dibari, C., Costafreda-Aumedes, S., Kartschall, T., Menz, C., Molitor, D., Junk, J., Beyer, M., Schultz, H.R., 2020. A Review of the Potential Climate Change Impacts and Adaptation Options for European Viticulture. Appl. Sci. 10, 3092. https://doi.org/10.3390/app10093092.
Sarri, D., Lombardo, S., Lisci, R., De Pascale, V., Vieri, M., 2020. AgroBot Smash a Robotic Platform for the Sustainable Precision Agriculture, in: Lecture Notes in Civil Engineering. Springer, pp. 793–801. https://doi.org/10.1007/978-3-030-39299-4_85.
Suárez, L., Zarco-Tejada, P.J., Berni, J.A.J., González-Dugo, V., Fereres, E., 2009. Modelling PRI for water stress detection using radiative transfer models. Remote Sens. Environ. 113, 730–744. https://doi.org/10.1016/j.rse.2008.12.001.
Suárez, L., Zarco-Tejada, P.J., Sepulcre-Cantó, G., Pérez-Priego, O., Miller, J.R., Jiménez-Muñoz, J.C., Sobrino, J., 2008. Assessing canopy PRI for water stress detection with diurnal airborne imagery. Remote Sens. Environ. 112, 560–575. https://doi.org/10.1016/j.rse.2007.05.009.
Testi, L., Goldhamer, D.A., Iniesta, F., Salinas, M., 2008. Crop water stress index is a sensitive water stress indicator in pistachio trees. Irrig. Sci. 26, 395–405. https://doi.org/10.1007/s00271-008-0104-5.
Thenot, F., Méthy, M., Winkel, T., 2002. The Photochemical Reflectance Index (PRI) as a water-stress index. Int. J. Remote Sens. 23, 5135–5139. https://doi.org/10.1080/01431160210163100.
Trout, T.J., Johnson, L.F., Gartung, J., 2008. Remote sensing of canopy cover in horticultural crops. HortScience 43, 333–337.
Tysseyre, B., Ojeda, H., Carillo, L., Deis, M.H., 2005. Precision viticulture and water status : mapping the predawn water potential to define within vineyard zones., in: 7th Fruit, Nut and Vegetable Production Engineering Symposium. Montpellier, France. Montpellier, France.
Van Zyl, J.L., 1986. Canopy Temperature as a Water Stress Indicator in Vines. South African J. Enol. Vitic. 7, 53–60. https://doi.org/10.21548/7-2-2326.
Williams, L.E., 2010. Grapevine water relations. Aust. J. Grape Wine Res. 16, A52–A62. https://doi.org/10.1111/j.1755-0238.2010.00083_5.x.
Williams, L.E., Ayars, J.E., 2005. Grapevine water use and the crop coefficient are linear functions of the shaded area measured beneath the canopy. Agric. For. Meteorol. 132, 201–211.
Yang, X., Liu, S., Liu, Y., Ren, X., Su, H., 2019. Assessing shaded-leaf effects on photochemical reflectance index (PRI) for water stress detection in winter wheat. Biogeosciences 16, 2937–2947. https://doi.org/10.5194/bg-16-2937-2019.
Zhang, C., Filella, I., Garbulsky, M., Peñuelas, J., 2016. Affecting Factors and Recent Improvements of the Photochemical Reflectance Index (PRI) for Remotely Sensing Foliar, Canopy and Ecosystemic Radiation-Use Efficiencies. Remote Sens. 8, 677. https://doi.org/10.3390/rs8090677.